

## A Benchmark Comparison of the Canadian Supercritical Water-cooled Reactor (SCWR) 64-element Fuel Lattice Cell Parameters using Various Computer Codes

**J. Sharpe<sup>1</sup>, F. Salaun<sup>1</sup>, D. Hummel<sup>1</sup>, A. Moghrabi<sup>1</sup>, M. Nowak<sup>1,2</sup>, J. Pencer<sup>1,3</sup>, D. Novog<sup>1</sup> and A. Buijs<sup>1</sup>**

<sup>1</sup> McMaster University, Ontario, Canada

([sharpejr@mcmaster.ca](mailto:sharpejr@mcmaster.ca))

<sup>2</sup> Institut National Polytechnique de Grenoble (Phelma), Grenoble, France

<sup>3</sup> Canadian Nuclear Laboratories, Ontario, Canada

### Abstract

Discrepancies in key lattice physics parameters have been observed between various deterministic (e.g. DRAGON and WIMS-AECL) and stochastic (MCNP, KENO) neutron transport codes in modeling previous versions of the Canadian SCWR lattice cell. Further, inconsistencies in these parameters have also been observed when using different nuclear data libraries. In this work, the predictions of  $k_{\infty}$ , various reactivity coefficients, and relative ring-averaged pin powers have been re-evaluated using these codes and libraries with the most recent 64-element fuel assembly geometry. A benchmark problem has been defined to quantify the dissimilarities between code results for a number of responses along the fuel channel under prescribed hot full power (HFP), hot zero power (HZP) and cold zero power (CZP) conditions and at several fuel burnups (0, 25 and 50 MW·d·kg<sup>-1</sup> [HM]). Results from deterministic (TRITON, DRAGON) and stochastic codes (MCNP6, KENO V.a and KENO-VI) are presented.

### 1. Introduction

The goal of this study was to quantify the discrepancies between various computer codes used in the analysis of the Canadian Pressure-tube SCWR (PT-SCWR) lattice fuel cell. This includes the deterministic neutron transport codes DRAGON and TRITON, and the stochastic neutron transport codes MCNP6, KENO V.a and KENO-VI. Burnup calculations were also performed using DRAGON, TRITON, and MCNP6 and compared at various burnups (0, 25 and 50 MW·d·kg<sup>-1</sup>[HM]).

It was previously shown that significant discrepancies between codes, including DRAGON, KENO V.a, KENO-VI, WIMS-AECL 3.1 and MCNP5 exist [1]. In [1], calculations of  $k_{\infty}$  were found to have a spread of  $\approx 16$  mk for exit burnup fuel, and CVR differences of up to 5 mk were found for fresh fuel. Similarly, disagreements of up to 9.46 mk were found between MCNP5 and WIMS-AECL under cold zero power conditions with fresh fuel and up to 12.65 mk with exit burnup fuel [2].

This study attempts to capture the differences between codes under the execution of a typical user having only knowledge of the problem geometry and thermalhydraulic conditions. Furthermore, if a certain code has burnup capabilities (i.e. DRAGON, TRITON, and MCNP6), that specific code was then used to perform burnup calculations and carry out the calculation of various responses at specific burnups (0, 25 and 50 MW·d·kg<sup>-1</sup>[HM]). For some codes, burnup calculations were not possible (i.e.

KENO V.a and KENO-VI<sup>1</sup>, so the number densities of all isotopes were taken from TRITON's burnup output.

A brief description of the different codes is given here.

## 1.1 DRAGON

DRAGON is a freely available code developed at École Polytechnique de Montréal that is capable of solving the neutron transport equation with burnup in two and three dimensions [3]. The collision probability method was used to solve for neutron flux over the problem geometry with an optimized spatial mesh that balanced computation time and accuracy. The specific code version employed was DRAGON 3.06Ld.

Two separate DRAGON models were created using two different nuclear data libraries: the freely available 172-group IAEA library in WIMSD format [4], and a 172-group ENDFB-VII.1 library freely distributed through École Polytechnique de Montréal in DRAGLIB format [5]. Both models used the same spatial mesh, thereby isolating the effect of nuclear data on the calculation. The IAEA library does not contain yttrium, so it was necessary to omit the isotope from the definition of the ceramic insulator material (the number density of zirconium and oxygen atoms remained conserved). The ENDFB-VII.1 library did include yttrium as well as resonance data for zirconium, allowing a resonance self-shielding cross section correction to be done on structural material in the lattice cell.

## 1.2 TRITON

All simulations performed by TRITON [6] employed the 238 energy group library based on ENDF/B-VII.0 that is included in the SCALE 6.1 [7] package. The multi-group transport equation solver (NEWT [8]) uses the discrete-ordinate method. Therefore, after a mesh-size sensitivity study, an optimized radial meshing on top of a Cartesian meshing was created and the order of the  $S_n$  level symmetric quadrature was set to 6.

Unlike LWRs, the positions of the pins in the Canadian SCWR concept are not in a regular square lattice. A Monte Carlo determination of Dancoff Factors (DFs) was thus necessary and performed with MCDANCOFF [9], which is also included in the SCALE package. DFs need to be evaluated apriori in order to have an accurate representation of the resonance self-shielded cross sections. Ideally, each fuel pin should have a unique DF, but pins located in the same ring have very similar DFs so an average value was calculated for each ring at each axial position for each set of conditions.

## 1.3 KENO-VI

Referred to as KENO238 throughout this study, KENO-VI [10] was used in the multigroup mode (238 energy group library based on ENDF/B-VII.0 included in the SCALE package) for simulation of the SCWR lattice cell. KENO-VI is part of the KENO Monte Carlo criticality program included in the

---

<sup>1</sup> It should be noted that KENO V.a and KENO-VI, in 238 groups, do have burnup capabilities through TRITON [6].

SCALE code package. KENO-VI uses an advanced and flexible geometry package known as the SCALE Generalized Geometry Package (SGGP) which provides KENO-VI with the capability to model any volume that can be constructed using quadratic equations. In KENO-VI, the Criticality Safety Analysis Sequence (CSAS6 [11]) provides automated problem-dependent processing of cross sections. CSAS6 calls and activates a set of sequences to provide resonance corrected cross sections in the resolved and unresolved resonance ranges. The default method (BONAMI [12]) was used in this study to provide corrected cross sections in the unresolved resonance range and CENTRM [13]/PMC [14] was used in the resolved resonance range (just as in NEWT). KENO-VI in multigroup mode then uses the processed cross sections for the flux calculation.

#### 1.4 KENO V.a

Referred to KENOCE throughout this study, KENO V.a [15] was used in the continuous energy mode with a set of libraries based on ENDF/B-VII.0. Performing the calculation in continuous energy removes the need to calculate Dancoff Factors and perform resonance self-shielding corrections of cross sections, thus simplifying calculations. KENO V.a is a Monte Carlo based code as well, tracking each neutron within the problem geometry from production to absorption.

A statistical uncertainty of  $\Delta k = \pm 0.00016$  was requested which was sufficient for calculations of coolant void reactivities and fuel temperature reactivity coefficients without introducing any large uncertainties. 3D cells were used, but lattices were effectively 2D as the 3<sup>rd</sup> dimension was uniform (along the vertical axis) for a 25 cm depth. All cell boundaries were reflective.

When calculating fuel temperature coefficients, it must be noted that temperature libraries were only available at 293 K, 600 K, 900 K, 1200 K and 2500 K, and no interpolation was performed by KENO V.a. For whatever material temperature is defined, the code will always use the closest available temperature in the library (e.g. if the fuel temperature is  $1200 \pm 100$  K, the code exclusively uses the data at 1200 K). Therefore, special care was taken to perturb fuel temperatures in Sect. 2.3.2.

#### 1.5 MCNP6

MCNP6 [16] is a Monte Carlo neutron transport code with the capability for isotopic depletion calculations via coupling to the evolution code CINDER90 [17] (previously implemented in MCNPX [18]).

For depletion, an initial transport calculation was performed at the beginning of each burnup step (step  $i$ ). Flux and reaction rates were then used to deplete the fuel half way through the next burnup step (step  $i+1/2$ ). A second transport calculation was then made: the resulting flux is taken as the average flux for the entire burnup step and is used for the final depletion calculation from step  $i$  to step  $i+1$ .

In order to ensure that all fission products' cross sections were evaluated at the right temperature, libraries for each position along the channel were generated with the code MAKXSf [19]. This code uses standard MCNP libraries in the ACE format and processes them into new libraries and XSDIR files at the desired temperatures. The resolved resonances are Doppler broadened using similar methods

to those used by the codes NJOY and DOPPLER [19]. It also interpolates thermal scattering data and unresolved resonance probability tables, thus assuring an optimal treatment of temperature effects on cross sections. Without this method, fission products' cross sections would be referenced at a temperature of 293.6 K, thus resulting in incorrect fuel temperature reactivity coefficient calculations as the fuel temperature always exceeds 1100 K.

Additionally, as fission products appear in the fuel, the computational time for each transport calculation increases (up to a factor of five or six). Moreover, accessing the interpolated libraries is much slower than accessing the default libraries provided with MCNP. It was necessary to choose reasonable criticality parameters as well as a reasonable number of burnup steps to make the study practical. Reference simulations for two positions were performed with 35 burnup steps (70 transport calculations). This was reduced to 23 steps making sure that the evolution of flux and important isotopic densities (Pu-239, Pa-233, U-233, Th-232...) remained comparable to those of the reference case. Also, if a large number of cycles were needed to achieve low uncertainty on  $k_{\infty}$ , fewer were required for the flux to converge (the flux is collapsed into 63 groups before being input into CINDER90).

## 2. Benchmark Specifications

### 2.1 Lattice Fuel Cell Geometry and Materials

The geometry for the most recent 64-element fuel assembly geometry can be seen diagrammatically in Figure 1 [20] (some details in [21]). The geometry is also 1/2, 1/4 and 1/8 cell symmetrical; hence, a degree of freedom was given to the users of the various codes. The thermalhydraulic conditions for various heights and burnups in the core are listed in the thermalhydraulics section.

### 2.2 Thermalhydraulic Conditions

#### 2.2.1 Hot Full Power

Hot full power calculations were performed at ten different axial positions, using thermalhydraulic conditions that are shown in Table 1 (determined by DRAGON coupled with CATHENA[22]), and at three different burnups: 0, 25 and 50 MW·d·kg<sup>-1</sup>[HM]. Hot Full Power at 0.0 MW·d·kg<sup>-1</sup> [HM] will be referred to HFP-0 for the rest of this document (likewise for the other two burnups).

#### 2.2.2 Hot Zero Power

For the case of HZP-0, all materials have a temperature of 600 K with an upward (outer) and downward (inner) coolant density of 0.59254 g·cm<sup>-3</sup>, with the exception of the moderator (density=1.0851 g·cm<sup>-3</sup>, temperature = 300 K) and the pressure tube temperature which is at 428.81 K. Since the coolant and other materials along the channel's length are the same, only one reference calculation was required here. HZP-25 and HZP-50 simulations, corresponding to 25 and 50 MW·d·kg<sup>-1</sup>[HM] respectively, were

also performed at  $h=0.75$  and  $h=4.75$  each. The exact compositions at the various burnups and axial positions can be requested from the corresponding author.

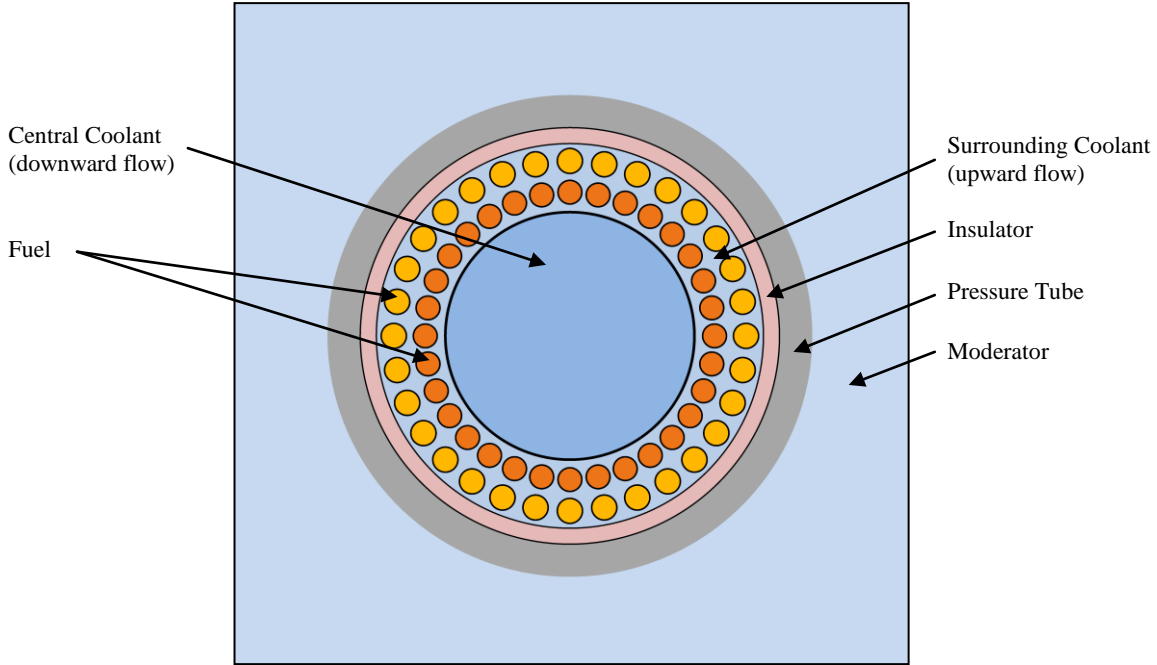


Figure 1: Cross-sectional view of the 64-element Canadian Pressure-tube SCWR.

Table 1: List of thermalhydraulic values used in this benchmark study. Densities are listed in  $\text{g}\cdot\text{cm}^{-3}$ , and temperatures in K.

<b>h (cm)</b>	$\rho_{\text{cool.}}$	$T_{\text{cool.}}$	$T_{\text{clad}}$	$T_{\text{liner}}$	$T_{\text{insul.}}$	$T_{\text{PT}}$	$T_{\text{centre}}$	$\rho_{\text{centre}}$	$T_{\text{fuel}}$
<b>0.25</b>	0.51702	647.40	683.04	640.78	537.68	410.38	636.45	0.57896	1117.36
<b>0.75</b>	0.40765	656.78	682.96	651.60	544.50	412.62	636.21	0.57998	1243.11
<b>1.25</b>	0.29633	660.87	682.12	655.72	547.08	413.47	635.81	0.58170	1321.80
<b>1.75</b>	0.21395	666.64	706.93	658.95	549.11	414.12	635.32	0.58374	1410.09
<b>2.25</b>	0.15946	680.69	752.43	669.19	555.52	416.20	634.74	0.58612	1504.15
<b>2.75</b>	0.12433	707.46	813.07	691.45	569.44	420.66	633.96	0.58932	1593.95
<b>3.25</b>	0.10151	747.28	878.78	726.60	591.28	427.56	632.80	0.59388	1662.50
<b>3.75</b>	0.08648	796.00	938.48	771.14	618.68	436.01	631.14	0.60025	1691.34
<b>4.25</b>	0.07651	846.57	984.39	818.38	647.79	444.77	628.83	0.60866	1660.86
<b>4.75</b>	0.07014	890.62	1006.99	859.82	673.29	452.28	625.81	0.61903	1539.91

### 2.2.3 Cold Zero Power

All materials have a temperature of 300 K with an upward and downward coolant density of  $0.996567 \text{ g}\cdot\text{cm}^{-3}$ , except the moderator (density =  $1.0851 \text{ g}\cdot\text{cm}^{-3}$ , temperature = 300 K). Since the coolant and

other materials along the channel's length are the same, only one reference calculation was required here. CZP-25 and CZP-50 simulations, corresponding to 25 and 50 MW·d·kg<sup>-1</sup>[HM] respectively, were also performed at h=0.75 and h=4.75.

## 2.3 Coolant Void Reactivity and Fuel Temperature Reactivity

### 2.3.1 Coolant Void Reactivity

An inner and outer coolant void reactivity (ICVR and OCVR) and total coolant void reactivity (TCVR) were requested, where coolant voided cases had coolant densities set to 0.001 g·cm<sup>-3</sup>.

### 2.3.2 Fuel Temperature Coefficient (FTC)

In order to account for differences in the FTC calculated above (FTC<sub>+</sub>) and below (FTC<sub>-</sub>) a reference temperature, the follow equation was used:

$$FTC_{avg} = \frac{FTC_{+} \left( \frac{1}{\Delta T_{+}} \right) + FTC_{-} \left( \frac{1}{\Delta T_{-}} \right)}{\frac{1}{\Delta T_{+}} + \frac{1}{\Delta T_{-}}} \quad (1)$$

Where  $\Delta T_{+/-}$  are the differences in temperature used to evaluate FTC<sub>+/-</sub>. In the case of using different temperature changes above and below the reference temperature, Eqn. (1) weights FTCs evaluated closer to the reference temperature higher than FTCs evaluated further from the reference temperature.

## 3. Results

### 3.1 Burnup

Depletion calculations were performed using DRAGON, TRITON and MCNP6. Two different cross sections libraries were used, separately, for the depletion calculation in DRAGON: The IAEA cross section library (DrIAEA), and the ENDF/B-VII.1 library (Dr7.1). **Figure 2** shows the  $k_{\infty}$  curve as a function of burnup for the four codes. After a burnup value of 0.1 MW·d·kg<sup>-1</sup>[HM] the curve becomes nearly linear for all the codes. DrIAEA, Dr7.1, MCNP6 and TRITON have 51, 51, 24 and 28 data points each, respectively, and are logarithmically separated, with many points at low burnup and few points at high burnup. The points were not shown on the graph to improve clarity. There are a different number of burnup steps in order to capture the differences between the users while performing calculations which they believe are correct.

Ten axial positions were simulated along the channel, all with trends similar to **Figure 2**, and are not shown here. Generally, MCNP6 consistently had the highest  $k_{\infty}$  amongst the four codes, at all the simulated axial positions, while DrIAEA constantly had the lowest  $k_{\infty}$ . Dr7.1 and TRITON had very similar values of  $k_{\infty}$ . It should be noted that TRITON and MCNP6 agree increasingly well as  $h \rightarrow 0.25$  m, the best agreement being  $\Delta\rho = 0.5$  mk at 0.0 MW·d·kg<sup>-1</sup> and 1.4 mk at 50 MW·d·kg<sup>-1</sup> at  $h = 0.25$  m.

The largest discrepancy between the entries at  $0.0 \text{ MW}\cdot\text{d}\cdot\text{kg}^{-1}$  is  $\Delta\rho = 10.1 \text{ mk}$  (with  $h = 4.25 \text{ m}$ ), and at  $50 \text{ MW}\cdot\text{d}\cdot\text{kg}^{-1}$  is  $\Delta\rho = 12.7 \text{ mk}$  (with  $h = 4.25 \text{ m}$ ), where the discrepancy remains fairly constant throughout the depletions, as can be seen in **Figure 2**.

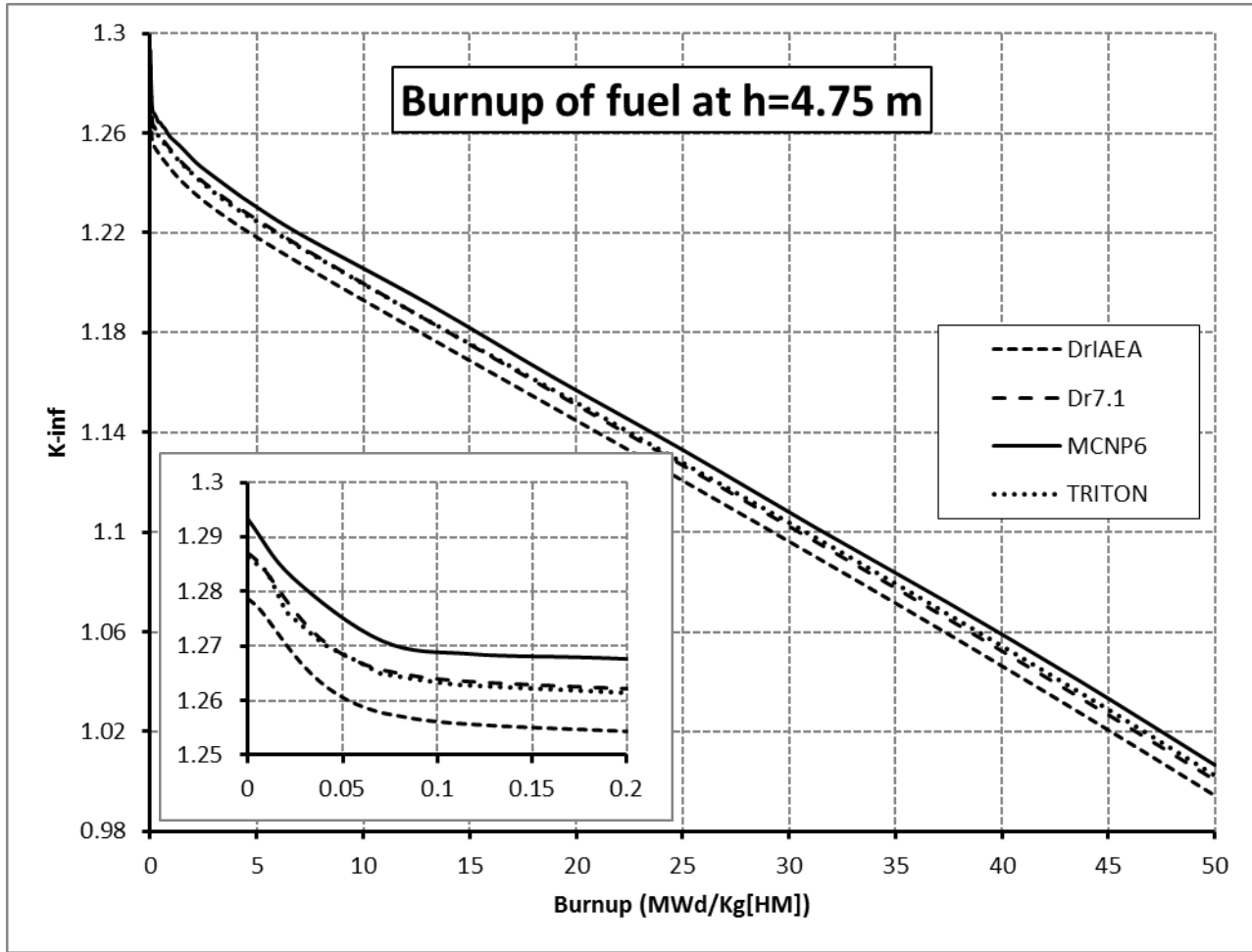


Figure 2:  $k_{\infty}$  versus burnup ( $\text{MW}\cdot\text{d}\cdot\text{kg}^{-1}[\text{HM}]$ ). The inset graph is a zoomed portion of the graph from  $0.0$  to  $0.2 \text{ MW}\cdot\text{d}\cdot\text{kg}^{-1}[\text{HM}]$ .

All curves plotted in Figure 3 to Figure 8 have data points only on the labelled x-axis grid lines (i.e.  $0.25 \text{ m}$ ,  $0.75 \text{ m}$ , ... ,  $4.75 \text{ m}$ ).

### 3.2 $k_{\infty}$

The multiplication constant was calculated by all six codes/libraries and is plotted in **Figure 3** as a function of axial height along the channel. Changes in fuel temperature and coolant density along the channel cause the fluctuations seen in the **Figure 3**.

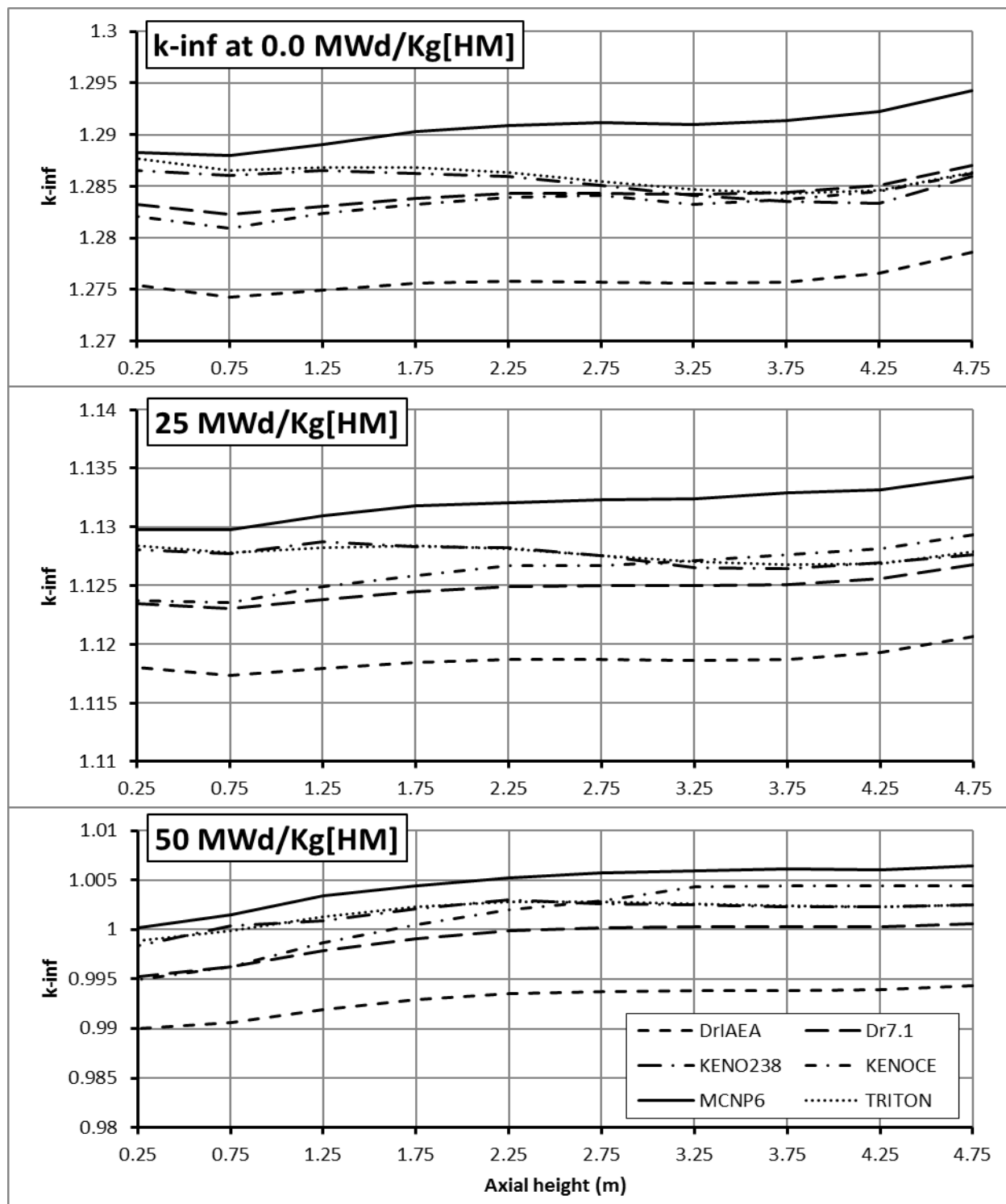


Figure 3:  $k_{\infty}$  plotted against axial height along the channel at various burnups.

As mentioned in Sect. 1.4, KENOCE, unlike the other codes, does not include any Doppler broadening calculations, nor does it interpolate between cross section libraries evaluated at given temperatures. In order to account for this the fuel temperature reactivity coefficient was incorporated in the  $k_{\infty}$  of KENOCE plotted in **Figure 3**.

There are two major variables at play between the bottom and the top of the channel. The fuel temperature increases, causing Doppler broadening of the resonances and reduces reactivity; meanwhile, the outer coolant becomes less dense as it picks up heat from the fuel. Due to the negative coolant density coefficient (as shown in Sect. 3.4 and Figure 5) along the channel, for all burnups, a positive insertion of reactivity takes place as outer density decreases. It is here that the negative fuel temperature reactivity coefficient and the negative outer coolant density coefficient can be seen.

As was seen in **Figure 2**, MCNP6 consistently has a higher  $k_{\infty}$  than the other codes, while DrIAEA has a consistently lower  $k_{\infty}$ . Generally speaking, TRITON and KENO238 are nearly identical at the three evaluated burnups while Dr7.1 and KENOCE exhibit similar behaviours. Also, the discrepancy between the codes slightly grows with increasing burnup, the largest being between DrIAEA and MCNP6 which have a difference of  $\approx 8$  mk at  $0 \text{ MW}\cdot\text{d}\cdot\text{kg}^{-1}$  and  $\approx 10$  mk at  $50 \text{ MW}\cdot\text{d}\cdot\text{kg}^{-1}$ .

### 3.3 Inner Coolant Void Reactivity (ICVR)

The downward central flow of light water within the SCWR channel (as seen in **Figure 1**) is referred to as the inner coolant throughout this paper, however it does not offer any appreciable amount of cooling while in the downward leg of the channel. Once the downward flow reaches the bottom of the channel it is forced outwards and up through the fuel region (outer coolant).

The ICVR trends, as seen in **Error! Reference source not found.**, for DrIAEA, Dr7.1, and TRITON are smooth and similar to that of MCNP6, however, KENO238 and KENOCE are outliers. KENO238 is not a smooth function of axial position within the 10 axial nodes that were chosen. This jagged curve can be explained by the statistical uncertainty in KENO238 simulations that was typically  $\approx 0.4$  mk, which would lead to an ICVR statistical uncertainty of roughly 0.6 mk. Also, note that the Doppler broadening of the calculated  $k_{\infty}$  was not included in these graphed values of KENOCE as this term would cancel in the CVR calculation.

### 3.4 Outer Coolant Void Reactivity (OCVR)

The flow of light water that passes upward by the fuel pins, collecting the heat and cooling the pins is referred to as the outer coolant. The OCVR is shown in **Figure 5**. There is only a small change in OCVR with burnup of  $\approx 2$  mk between 0 and  $50 \text{ MW}\cdot\text{d}\cdot\text{kg}^{-1}$ , however, there is a decrease in OCVR with increasing height along the channel that is consistent with all the codes. The decrease in OCVR with increasing height is due to the decrease in reference outer coolant density with increasing height. Near the top of the channel a relatively small amount of coolant is lost between the reference (shown in **Table 1**) and voided conditions, whereas at the bottom of the channel there is a larger amount of coolant lost.

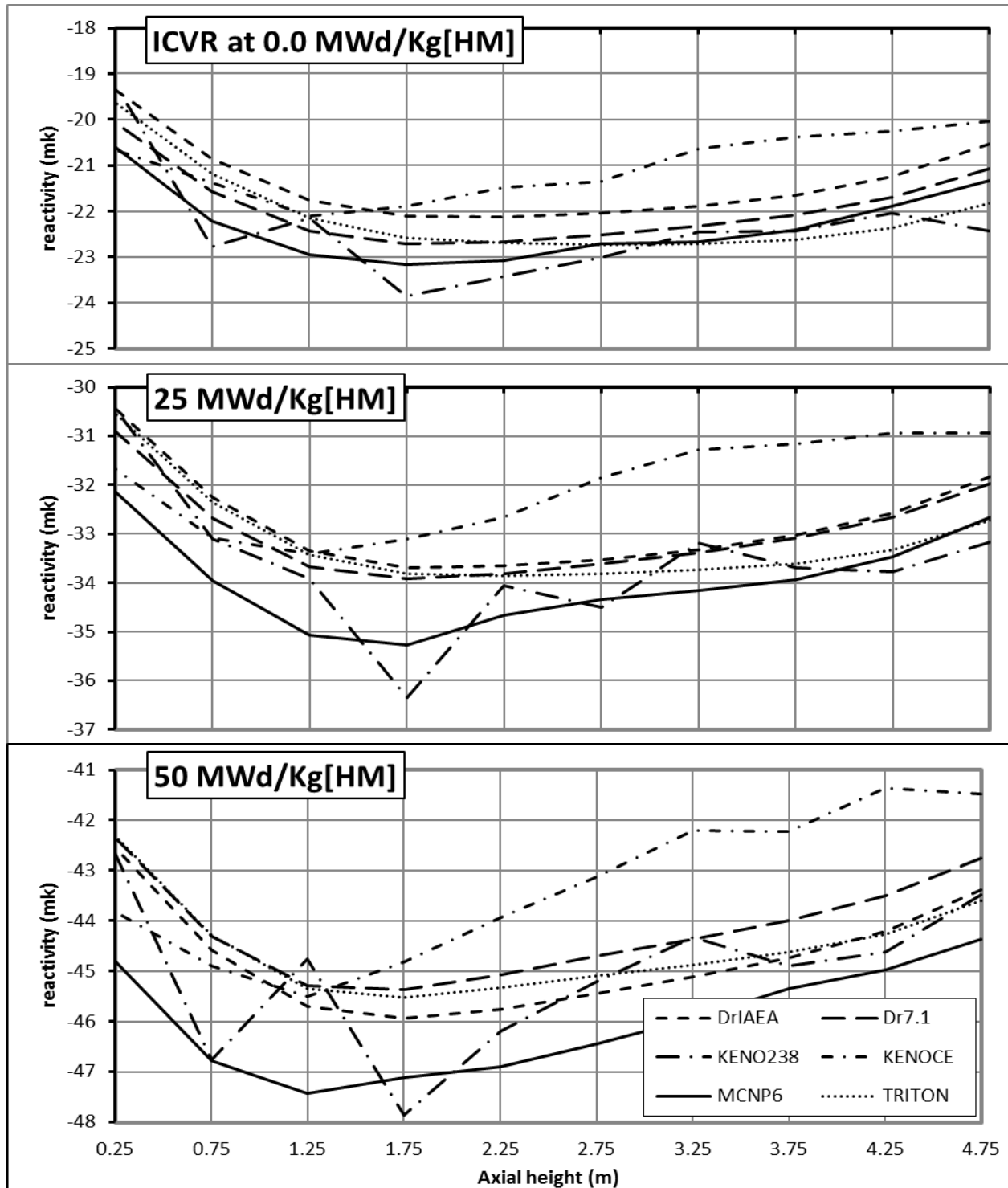


Figure 4: Inner Coolant Void Reactivity (ICVR) along the vertical axis of an SCWR fuel channel at various burnups.

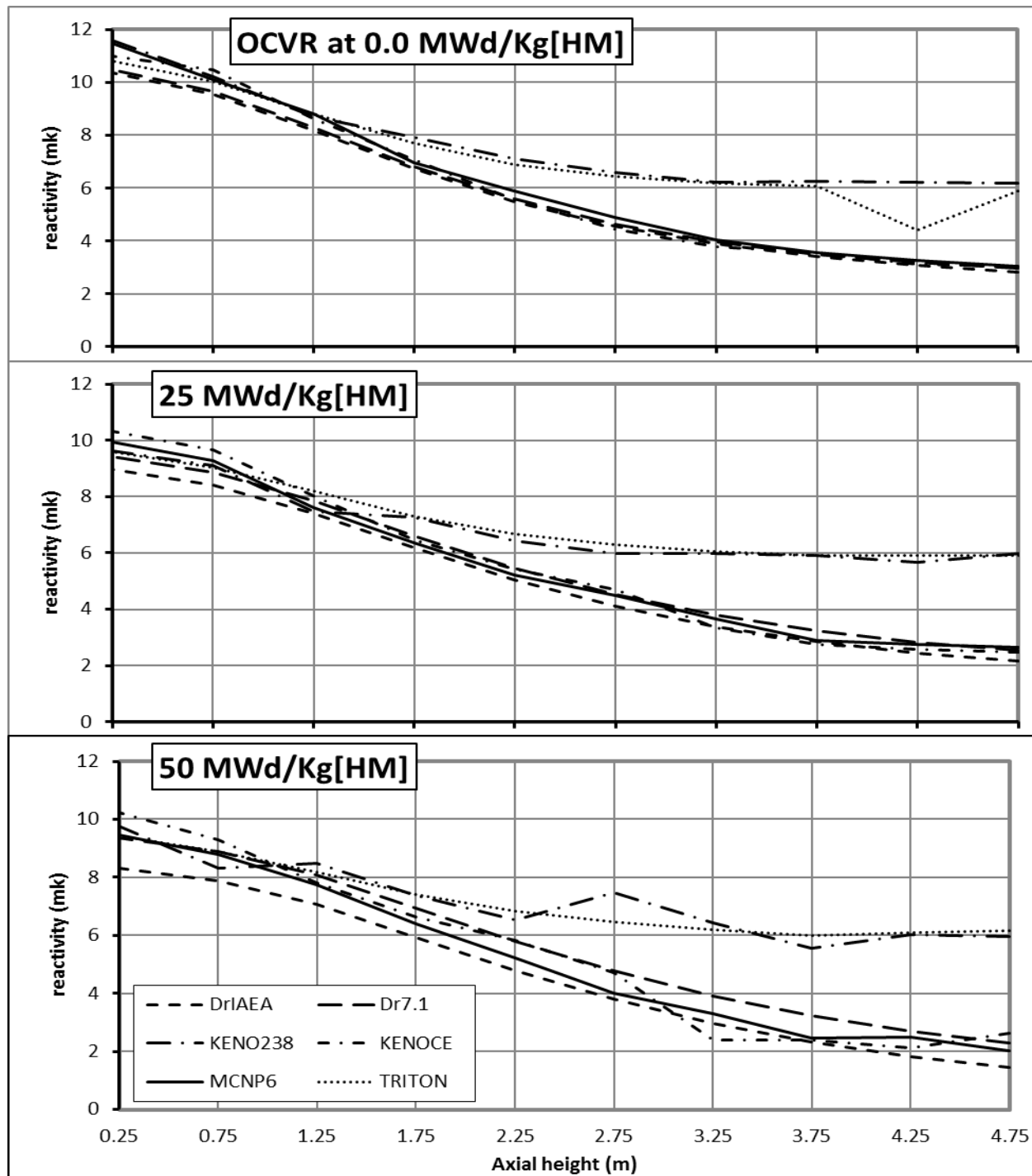


Figure 5: Outer Coolant Void Reactivity (OCVR) along the vertical axis of an SCWR fuel channel at various burnups.

KENO238 and TRITON are the outliers in these plots, which do not decrease as much as the other codes as height increases, however, in general the other codes agree very well at all burnups and axial positions. Please note that **Error! Reference source not found., Figure 5** and **Figure 6** do not use the same vertical scale.

### 3.5 Total Coolant Void Reactivity (TCVR)

The total coolant void reactivity is plotted in **Figure 6**. This condition has been simulated by all the codes (having the inner and outer coolant voided), and is not simply the sum of the ICVR and OCVR. All codes exhibit similar overall behaviour along the channel, having a decreasing TCVR with increasing axial position, however, KENOCE is constantly above the other codes by  $\approx 1$  mk,  $\approx 2$  mk and  $\approx 3$  mk, at 0, 25 and 50 MW·d·kg<sup>-1</sup>, respectively. Please note that **Error! Reference source not found., Figure 5** and **Figure 6** do not use the same vertical scale.

### 3.6 Fuel Temperature Coefficient (FTC)

The fuel temperature coefficient as a function of axial position along an SCWR channel is plotted below in **Figure 7**, at various burnups. The curve follows a negative quadratic like shape along the channel, with a peak near  $h=3.75$  m at all burnups.

MCNP6 displays fairly erratic behaviour but this is not believed to be due to statistical uncertainties which are below  $\pm 0.04$  pcm·K<sup>-1</sup> at all burnups. KENO238 displays irregular behaviour at the bottom of the channel, this is due to a simulated fuel temperature difference of 300 K which led to an uncertainty of 0.21 pcm/K for  $h=0.25$  m (0.16 pcm·K<sup>-1</sup> at 25 MW·d·kg<sup>-1</sup> and 0.13 pcm·K<sup>-1</sup> at 50 MW·d·kg<sup>-1</sup>), however for all other positions along the channel (i.e.  $h \neq 0.25$  m), the uncertainty is below 0.07 pcm/K, at all burnups, due to a temperature difference of 1300 K in the cross section libraries. Conversely, KENOCE has a statistical uncertainty of less than 0.013 pcm·K<sup>-1</sup> at all burnups and positions. It is not immediately clear why there are large variations in the FTC for MCNP6 at all burnups, although the variations may be attributable to the cross section interpolation method that was used between libraries at different temperatures.

### 3.7 Relative Power Ratio (O/I)

The relative power ratio is the ratio of the outer-to-inner ring-totalled pin powers and has been plotted in Figure 8. O/I has been calculated by summing the total outer ring power and dividing by the total inner ring power, and is abbreviated O/I throughout this paper (to signify outer over inner ring power). O/I decreases slowly with burnup, and decreases with increasing height along the channel. The codes produce very similar results, all within 2% of each other, at all burnups. TRITON slowly migrates upwards with respect to the other codes with increasing burnup and MCNP6 seems to predict a slightly higher than average O/I (other than TRITON) at all burnups, compared to the other codes. The scale of the y-axis in all of the panes of Figure 8 are the same, this allows an easy comparison of discrepancy of the codes.

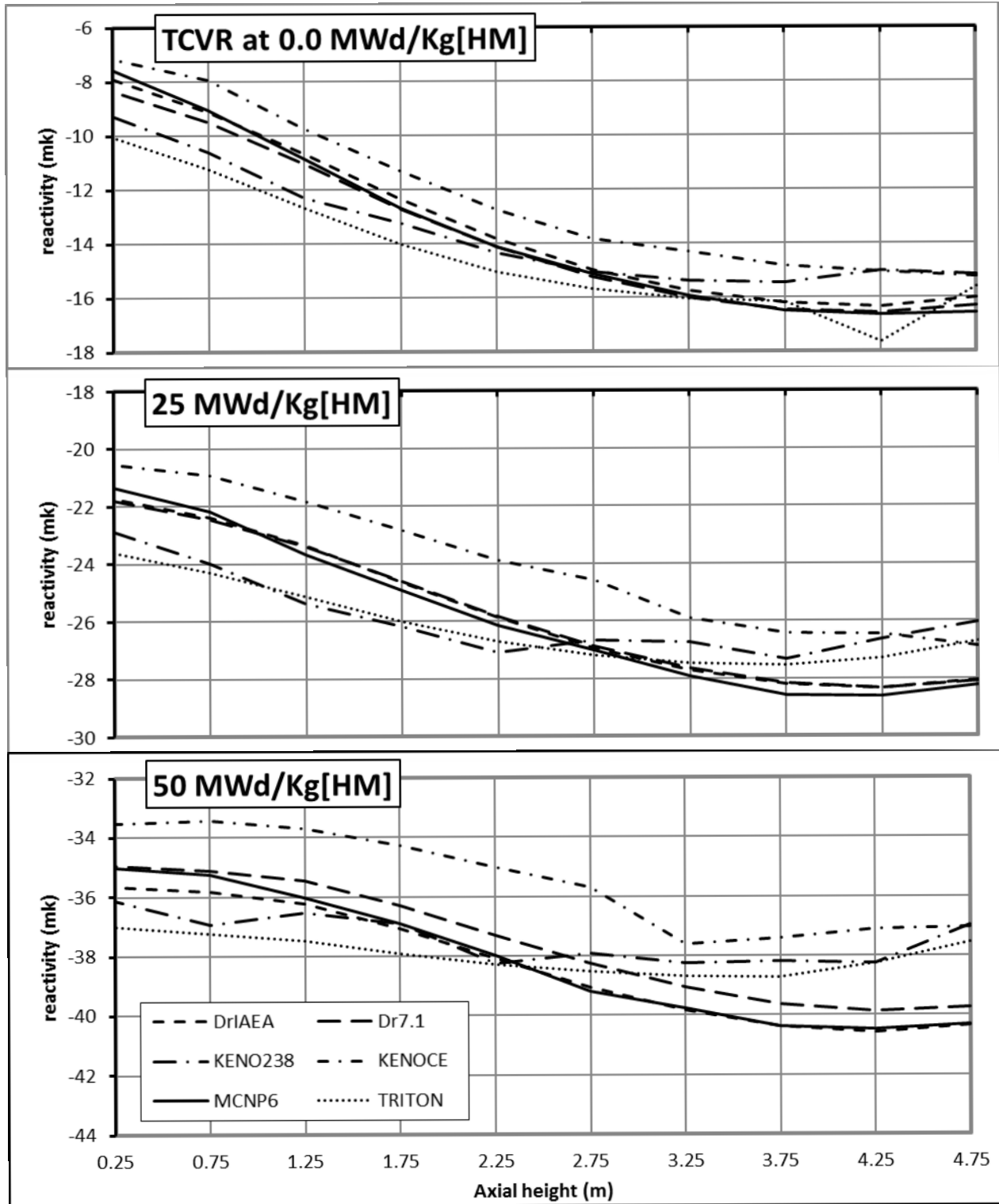


Figure 6: Total Coolant Void Reactivity (TCVR) along the vertical axis of an SCWR fuel channel at various burnups.

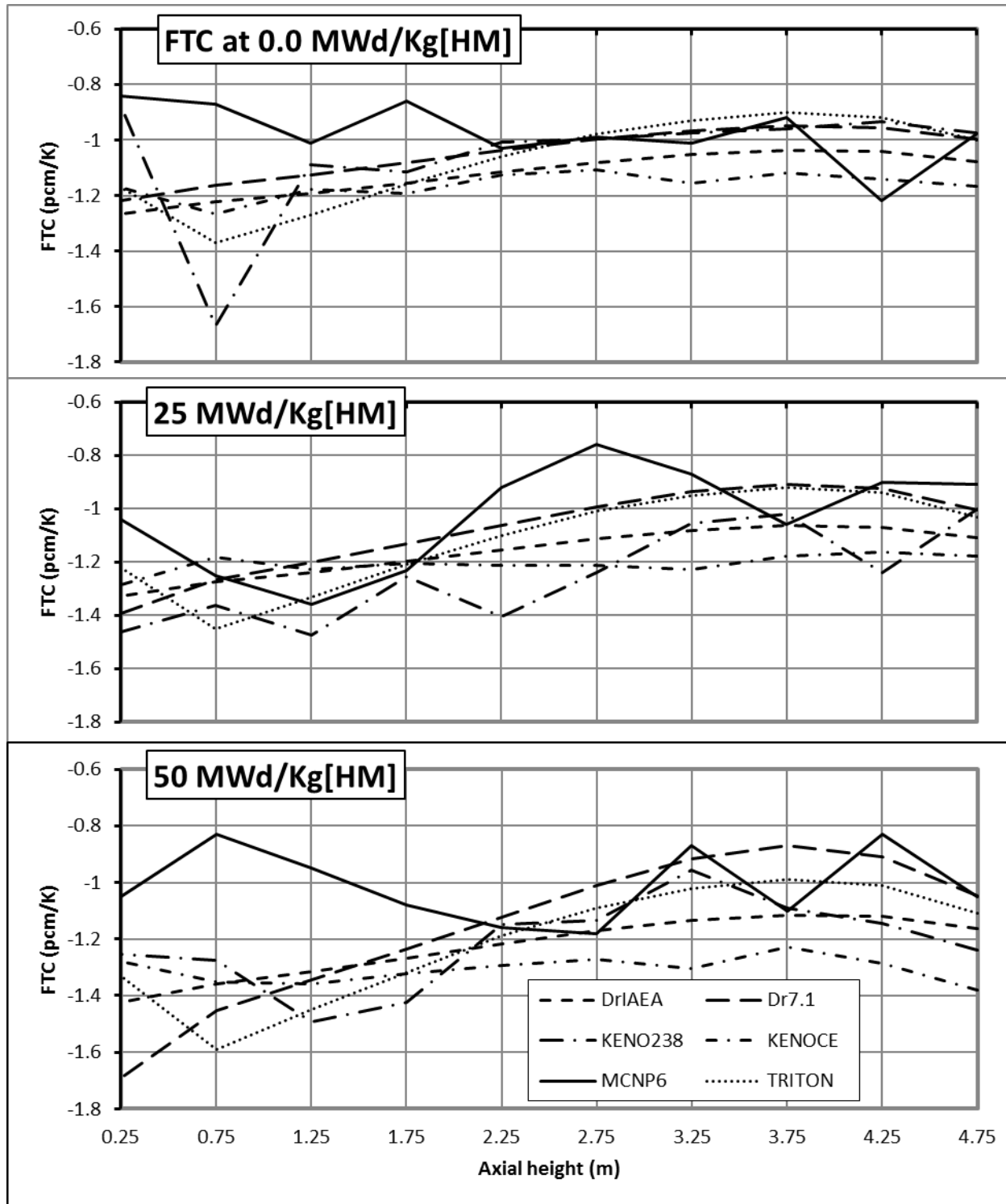


Figure 7: Fuel Temperature Coefficient (FTC) as a function of axial position along an SCWR channel at various burnups. Please see Sect. 3.6 regarding additional uncertainty information, however, error bars have been omitted from this graph for clarity.

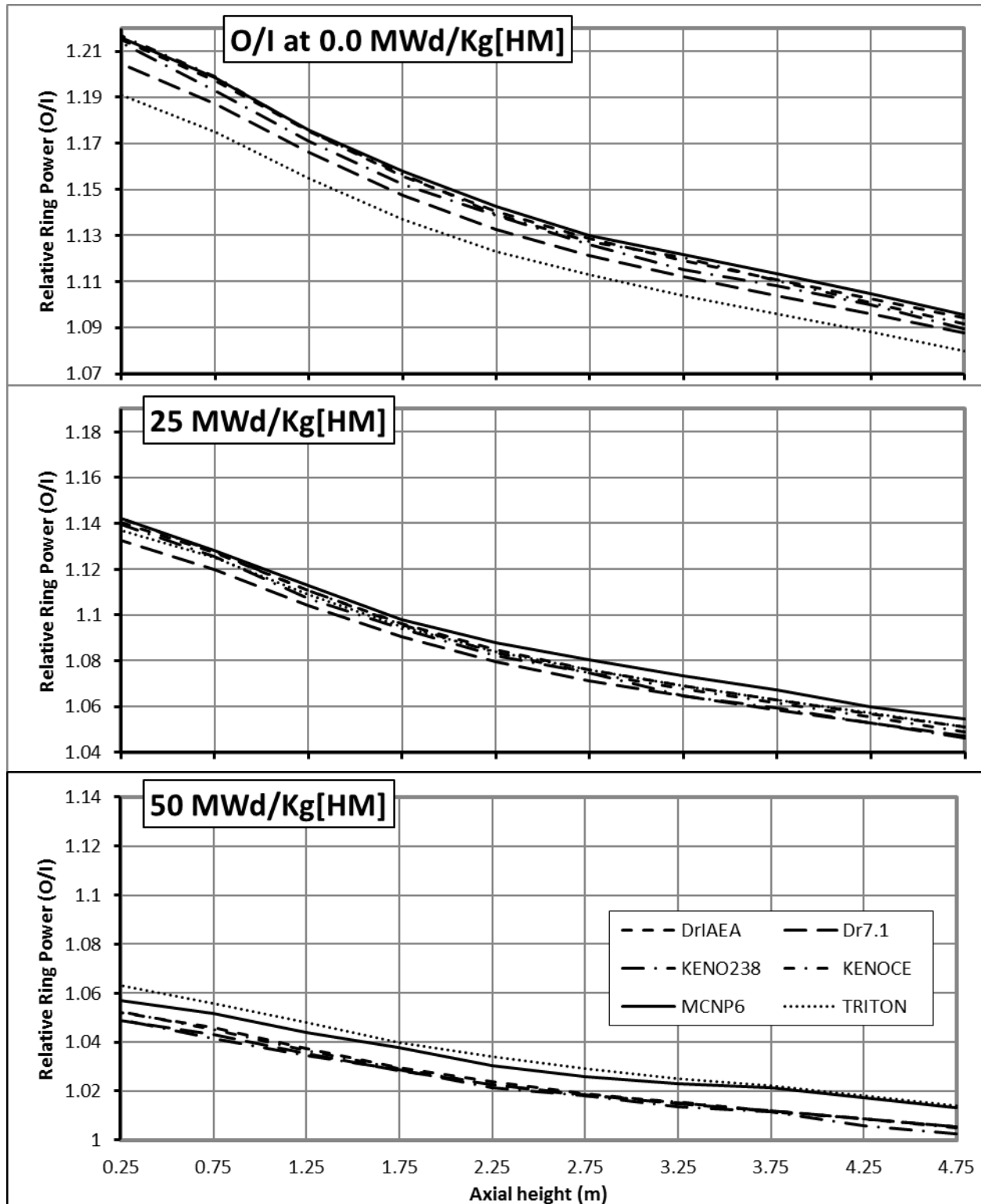


Figure 8: Outer-to-inner ring-totaled power ratio along an SCWR channel at various burnups.

### 3.9 Cold Zero Power (CZP)

The cold zero power conditions displayed in **Table 2** show that the different codes agree fairly well at 0 MW·d·kg<sup>-1</sup> burnup, but the discrepancies typically grow with burnup. KENO238 routinely has larger values for voided cases compared to the other codes, and also has a relatively small FTC compared to the other codes. The trends for  $k_{\infty}$  are not similar to those seen in **Figure 3**, and in this case TRITON displays some of the largest  $k_{\infty}$ . However, there is similarity with regards to the O/I ring power between Figure 8 and **Table 2**, that O/I decreases with burnup.

Table 2: Various responses under cold zero power conditions at various burnups.

<b>CZP</b>	<b>Burnup (MW·d·kg<sup>-1</sup>)</b>	<b>DrIAEA</b>	<b>Dr7.1</b>	<b>KENO238</b>	<b>KENOCE</b>	<b>MCNP6</b>	<b>TRITON</b>
<b>k<sub>∞</sub></b>	<b>0</b>	1.20073	1.20852	1.20530	1.20176	1.20929	1.21160
	<b>25</b>	1.04056	1.04621	1.04395	1.04047	1.04788	1.04879
	<b>50</b>	0.91024	0.91622	0.91342	0.90993	0.91585	0.91596
<b>ICVR (mk)</b>	<b>0</b>	49.0	47.7	50.4	49.7	48.6	47.1
	<b>25</b>	53.4	51.9	54.4	54.5	52.7	51.2
	<b>50</b>	58.5	56.7	58.2	59.7	57.9	56.3
<b>OCVR (mk)</b>	<b>0</b>	13.7	13.6	15.0	14.9	14.9	15.0
	<b>25</b>	16.1	16.0	17.7	18.5	18.1	17.9
	<b>50</b>	21.2	21.2	22.4	24.2	24.1	23.8
<b>TCVR (mk)</b>	<b>0</b>	58.4	57.2	60.0	62.3	60.3	55.4
	<b>25</b>	63.3	62.3	64.7	69.4	66.3	60.6
	<b>50</b>	72.6	71.6	74.3	81.4	77.3	70.5
<b>FTC (pcm·K<sup>-1</sup>)</b>	<b>0</b>	-2.26	-2.21	-1.21	-1.83	-2.24	-2.39
	<b>25</b>	-2.46	-2.43	-1.16	-1.92	-2.45	-2.65
	<b>50</b>	-2.75	-2.70	-1.72	-2.37	-2.83	-3.06
<b>O/I</b>	<b>0</b>	1.19	1.18	1.19	1.20	1.19	1.17
	<b>25</b>	1.13	1.12	1.14	1.14	1.14	1.12
	<b>50</b>	1.06	1.06	1.06	1.07	1.07	1.05

### 3.10 Hot Zero Power (HZP)

Hot zero power conditions are shown in **Table 3**. Regarding  $k_{\infty}$ , the results are similar to those in **Figure 3**, except that TRITON no longer falls below the other codes at all burnups, but rather lies in the middle of the other codes. ICVR becomes increasingly negative for all codes with burnup while OCVR is rather constant at all burnups between all the codes. There is an apparent superposition that occurs between ICVR and OCVR to produce the TCVR results which also becomes increasingly negative with burnup. With respect to FTC, MCNP6 is showing results outside the norm (as was found with the FTC at hot full power), in this case being below the other codes at all burnups. Finally, O/I decreases monotonically, between all codes, with increasing burnup.

Table 3: Various responses under hot zero power conditions at various burnups.

<b>HZP</b>	<b>Burnup (MWd/Kg)</b>	<b>DrIAEA</b>	<b>Dr7.1</b>	<b>KENO238</b>	<b>KENOCE</b>	<b>MCNP6</b>	<b>TRITON</b>
<b>k<sub>∞</sub></b>	<b>0</b>	1.28497	1.29273	1.29494	1.29032	1.29727	1.29498
	<b>25</b>	1.12463	1.13023	1.13161	1.12915	1.13468	1.13248
	<b>50</b>	0.99451	1.00042	0.99994	0.99808	1.00025	1.00011
<b>ICVR (mk)</b>	<b>0</b>	-15.03	-15.75	-16.28	-15.80	-16.51	-15.66
	<b>25</b>	-24.83	-25.60	-24.96	-25.48	-26.84	-25.50
	<b>50</b>	-35.48	-36.13	-36.22	-35.77	-35.63	-36.04
<b>OCVR (mk)</b>	<b>0</b>	11.02	11.08	11.62	12.07	11.92	11.83
	<b>25</b>	9.92	10.11	11.36	11.30	11.32	10.91
	<b>50</b>	9.79	10.09	11.37	12.38	13.87	11.16
<b>TCVR (mk)</b>	<b>0</b>	-4.40	-4.89	-5.83	-2.88	-4.28	-6.43
	<b>25</b>	-16.93	-17.21	-18.27	-14.50	-16.19	-19.03
	<b>50</b>	-29.22	-29.10	-30.59	-24.70	-25.80	-31.25
<b>FTC (pcm/K)</b>	<b>0</b>	-1.79	-1.67	-1.96	-1.69	-1.49	-1.77
	<b>25</b>	-1.89	-1.77	-1.85	-1.91	-1.92	-1.90
	<b>50</b>	-2.05	-1.93	-2.24	-2.07	-1.74	-2.13
<b>O/I</b>	<b>0</b>	1.22	1.21	1.21	1.22	1.22	1.19
	<b>25</b>	1.14	1.14	1.15	1.15	1.15	1.13
	<b>50</b>	1.06	1.05	1.06	1.06	1.06	1.06

#### 4. Discussion

It is emphasised that this work has been performed to demonstrate the difference between codes that have been completely independently developed, using different: meshing (for the deterministic codes), neutrons per cycle, number of cycles (stochastic codes), burnup steps and other parameters. The users of each code have deemed that the parameters they used were adequate and the differences between the codes presented in this paper capture those expected differences, along with library and code differences. These user differences are to be expected when comparing results of different codes between different users at different companies, laboratories and universities.

#### 5. Conclusion

With regards to burnup, DrIAEA, Dr7.1, MCNP6, TRITON, all exhibit the same trends in k<sub>∞</sub>, however fairly large discrepancies of up to ≈10 mk can lead to significantly shorter or longer cycle lengths. Based on this result, optimization of a refuelling scheme, control device design and reactivity hold down mechanism designs will be sensitive to the specific code and/or nuclear data library used in any constituent lattice calculations.

MCNP5 is widely used in the reactor physics community as a benchmark tool because of its accuracy [1]. That said, within this study, under the various conditions, in general there are no codes that

consistently give results similar to MCNP6. However, under specific conditions, different codes perform well (or are comparable to MCNP6).

In terms of trends, here are the codes that perform similar to that of MCNP6, under the various conditions:

- $k_{\infty}$ : DrIAEA, Dr7.1, KENOCE
- ICVR: DrIAEA, Dr7.1, TRITON
- OCVR: DrIAEA, Dr7.1, KENOCE
- TCVR: DrIAEA, Dr7.1
- O/I: All codes

The authors suggest that FTC not be considered for comparison with MCNP6, as it is not immediately clear why large differences exist between MCNP6 and all other codes, while the other codes agree quite well amongst themselves.

In terms of the smallest differences between in value predicted by MCNP6, under the various conditions:

- $k_{\infty}$ : KENO238, TRITON
- ICVR: KENO238
- OCVR: DrIAEA, Dr7.1, KENOCE
- TCVR: DrIAEA, Dr7.1
- O/I: All codes

It should be further pointed out that using the same cross section based libraries (i.e. ENDF/B-VII.1) in codes (other than MCNP6) does not necessarily produce the most comparable results to MCNP6, additionally, codes using older libraries based on ENDF/B-VII.0, under certain conditions, may produce better results than ENDF/B-VII.1 based codes/libraries, when compared to MCNP6. Moreover, stochastic KENOCE and KENO238 do not regularly produce better results than the deterministic codes, and more importantly DrIAEA repeatedly performs well in comparison to MCNP6.

The authors suggest that further investigation into why these code differences exist, and suggestions on how to improve these codes should be made to the code developers.

## 6. References

- [1] D.W. Hummel, S.E. Langton, M.R. Ball, D.R. Novog and A. Buijs, “Description and Preliminary Results of a Two-Dimensional Lattice Physics Code Benchmark for the Canadian Pressure Tube Supercritical Water-cooled Reactor (PT-SCWR)” in *6<sup>th</sup> International Symposium on Supercritical Water-Cooled Reactors (ISSCWR-6)*, Shenzhen, China, 2013.
- [2] J. Pencer and L. Blomeley, “A Preliminary SCWR 2D Lattice-level Benchmark Comparison of WIMS-AECL and MCNP”, Atomic Energy of Canada Ltd., Chalk River, Canada, Gen. Rep. 217-123700-REPT-005 Rev. 0. (FFC-RRP-2084), Jan. 2013.

- [3] G. Marleau, A. Hébert and R. Roy, “A User Guide for DRAGON 3.06”, Institut de génie nucléaire, Département de génie physique, École Polytechnique de Montréal, Montréal, 2008.
- [4] International Atomic Energy Agency, “WIMS Library Update Project,” 28 January 2008. [Online]. Available: <http://www-nds.iaea.org/wimsd>. [Accessed 29 October 2012].
- [5] École Polytechnique de Montréal, “Draglib Download Page”, 5 May 2008. [Online]. Available: <http://www.polymtl.ca/merlin/libraries>. [Accessed 31 December 2014].
- [6] M.A. Jessee and M.D. Dehart, “TRITON: A Multipurpose Transport, Depletion, and Sensitivity and Uncertainty Analysis Module,” Tech. Rep. ORNL/TM-2005/39 Version 6.1 Sect. T1, Oak Ridge National Laboratory, June 2011.
- [7] SCALE 6.1. Radiation Safety Information Computational Center. <https://rsicc.ornl.gov>, 2013.
- [8] M.A. Jessee and M.D. DeHart, “NEWT: A New Transport Algorithm for Two-Dimensional Discrete-Ordinates Analysis in Non-Orthogonal Geometries,” Tech. Rep. ORNL/TM-2005/39 Version 6.1 Sect. F21, Oak Ridge National Laboratory, June 2011.
- [9] L.M. Petrie and B.T. Rearden, “MCDANCOFF Data Guide,” Tech. Rep. ORNL/TM-2005/39 Version 6.1 Sect. M24, Oak Ridge National Laboratory, June 2011.
- [10] D.F. Hollenbach, L. M. Petrie, S. Goluoglu, N.F. Landers and M.E. Dunn, “KENO-VI: A General Quadratic Version of the KENO Program,” Tech. Rep. ORNL/TM-2005/39 Version 6.1 Sect. F17, Oak Ridge National Laboratory, June 2011.
- [11] S. Goluoglu, D.F. Hollenbach and L.M. Petrie, “CSAS6: Control Module for Enhanced Criticality Safety Analysis with KENO-VI,” Tech. Rep. ORNL/TM-2005/39 Version 6.1 Sect. C6, Oak Ridge National Laboratory, June 2011.
- [12] N. M. Greene, “BONAMI, Resonance Self-Shielding by the Bondarenko Method,” Tech. Rep. ORNL/TM-2005/39 Version 6.1 Sect. F1, Oak Ridge National Laboratory, June 2011.
- [13] M.L. Williams and D.F. Hollenbach, “CENTRM: A One-dimensional Neutron Transport Code for Computing Pointwise Energy Spectra,” Tech. Rep. ORNL/TM-2005/39 Version 6.1 Sect. F18, Oak Ridge National Laboratory, June 2011.
- [14] M.L. Williams and D.F. Hollenbach, “PMC: A Program to Produce Multigroup Cross Section Using Pointwise Energy Spectra from CENTRM,” Tech. Rep. ORNL/TM-2005/39 Version 6.1 Sect. F19, Oak Ridge National Laboratory, June 2011.
- [15] L.M. Petrie, N.F. Landers, D.F. Hollenbach, B.T. Rearden, M.E. Dunn and S. Goluoglu, “KENO V.a: An Improved Monte Carlo Criticality Program,” Tech. Rep. ORNL/TM-2005/39 Version 6.1 Sect. F11, Oak Ridge National Laboratory, June 2011.
- [16] “MCNP6 User’s Manual Version 1.0”, LA-CP-13-00634, Rev.0, Los Alamos National Laboratory, May 2013.
- [17] W. B. WILSON et al., “Recent Development of the CINDER’90 Transmutation Code and Data Library for Actinide Transmutation Studies”, LA-UR-2181, Los Alamos National Laboratory Report (1995).
- [18] Forrest B. Brown, “The MAKXS F Code with Doppler Broadening”, LA-UR-06-7002, Los Alamos National Laboratory.

- [19] M.L. Fensin, “Development of the MCNPX Depletion Capability: A Monte Carlo Linked Depletion Method that automates the coupling between MCNPX and Cinder90 for high fidelity burnup calculations”, University of Florida, 2008.
- [20] J. Pencer, D. Watts, A. Colton, X. Wang, L. Blomeley, V. Anghel and S. Yue, “Core Neutronics for the Canadian SCWR Conceptual Design,” *In the 6<sup>th</sup> International Symposium on Supercritical Water-cooled Reactors (ISSCWR-6)*, Shenzhen, Guangdong, China, 2013, Submission 21.
- [21] J. Pencer, M. McDonald and V. Anghel, “Parameters for Transient Response Modelling for the Canadian SCWR,” *In 19<sup>th</sup> Pacific Basin Nuclear Conference (PBNC-2014)*, Vancouver, BC, Canada, 2014, Submission 403.
- [22] B.N. Hanna, “CATHENA: A thermal-hydraulic code for CANDU analysis”, *Nuclear Engineering and Design*, **180** (1998) 113-131.